Supplementary Information

Mechanically Encoded Strain-Vector Keys as Physical Unclonable Function

*Ji-Hoon Choi[a], Ji-Yea Lee[a], Sin-Hyung Lee[*b], and Hea-Lim Park[*a]*

[a]Department of Materials Science and Engineering, Seoul National University of Science and Technology, Seoul 01811, Republic of Korea

[b]School of Advanced Fusion Studies, Department of Intelligent Semiconductor Engineering, University of Seoul, 163 Seoulsiripdaero, Dongdaemun-gu,

Seoul, 02504, Republic of Korea

E-mail: sinhlee@uos.ac.kr (S.-H. Lee), parkhl21@seoultech.ac.kr (H.-L. Park)

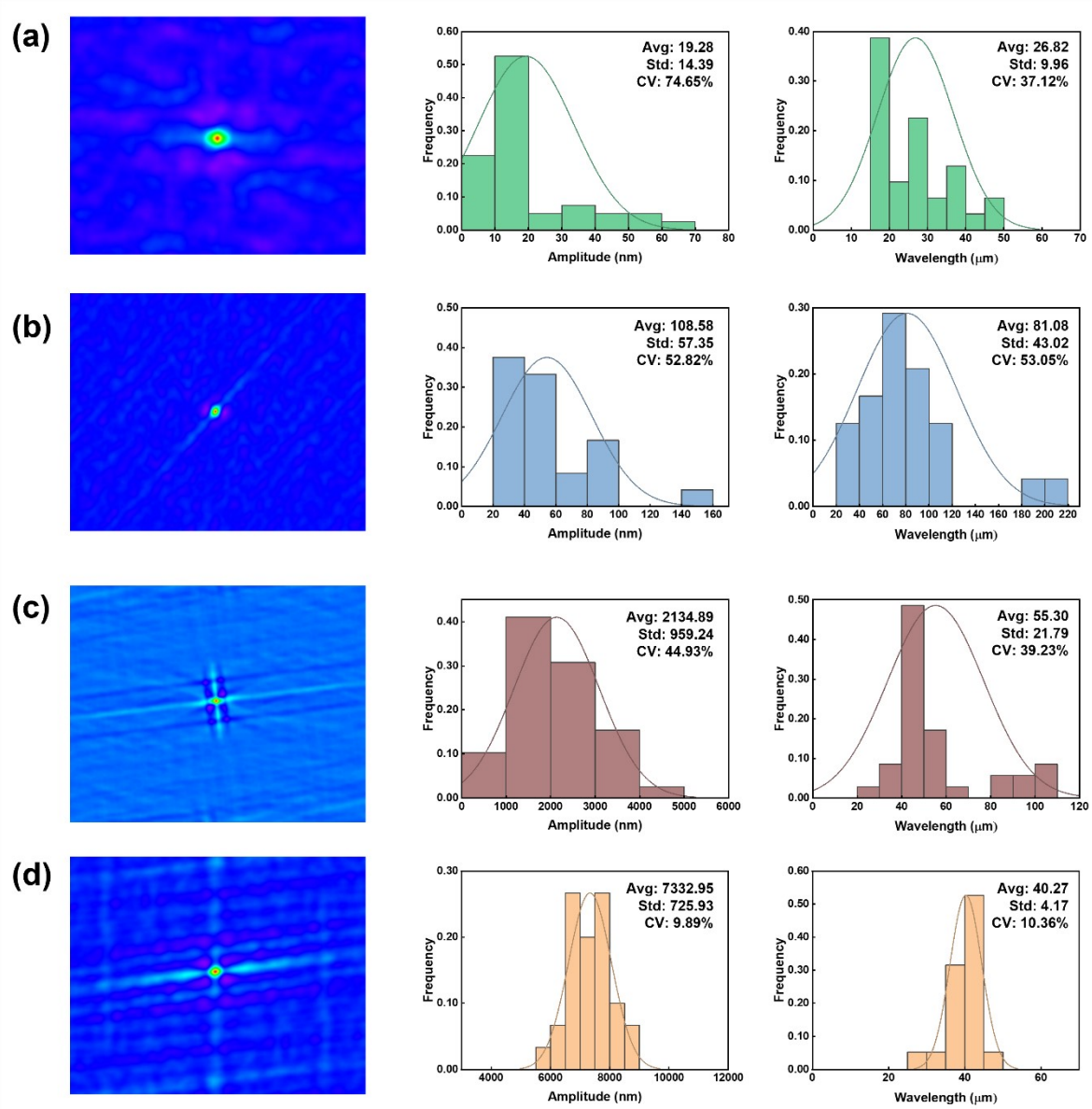

Fig. S1 Ultraviolet ozone (UVO)-time-dependent wrinkle analysis using 2D autocorrelation maps, amplitude histograms, and wavelength (spatial period) histograms for samples treated for (a) 5 min, (b) 10 min, (c) 20 min, and (d) 30 min.

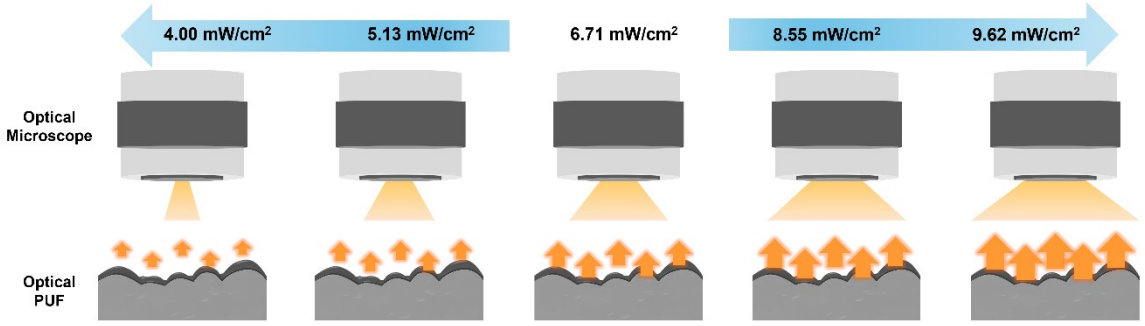

Fig. S2 Schematic illustration of optical PUF measurements under diverse illumination conditions.

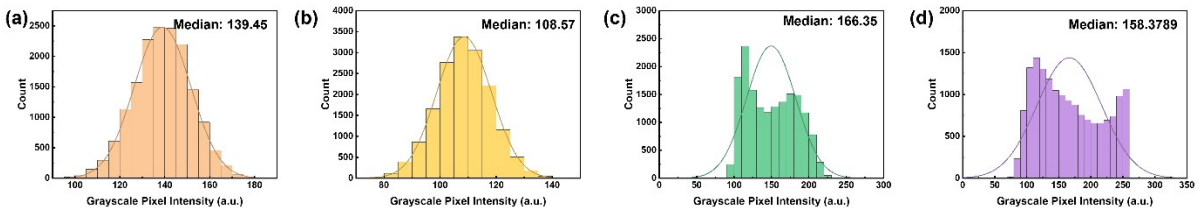

Fig. S3 Grayscale pixel-intensity histograms as a function of UVO treatment time: (a) 5 min, (b) 10 min, (c) 20 min, and (d) 30 min.

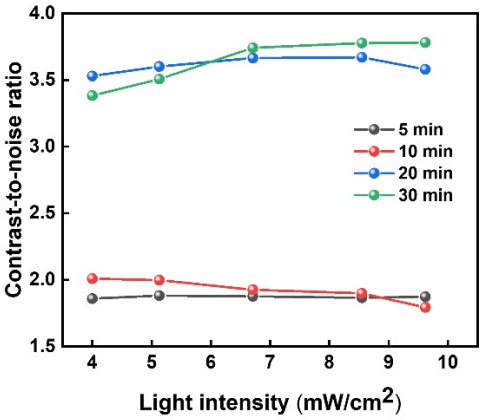

Fig. S4 Contrast-to-noise ratio (CNR) between the "0" and "1" signals (median-based binarization) measured as a function of readout light intensity for optical PUF samples prepared with different UVO treatment times (5, 10, 20, and 30 min).

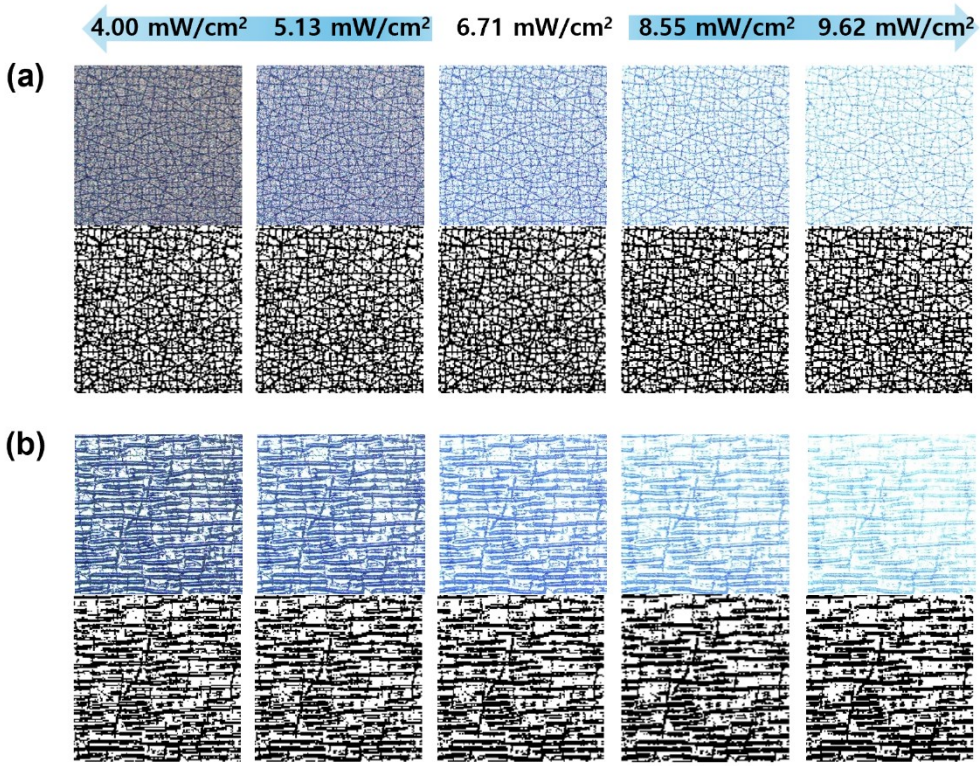

Fig. S5 (a) Optical microscopy (OM) and digital images according to x-axis tensile strain (0–30%) for the ultra-violet ozone (UVO) 20 min sample. (b) OM and digital images according to x-axis tensile strain (0–30%) for the UVO 30 min sample.

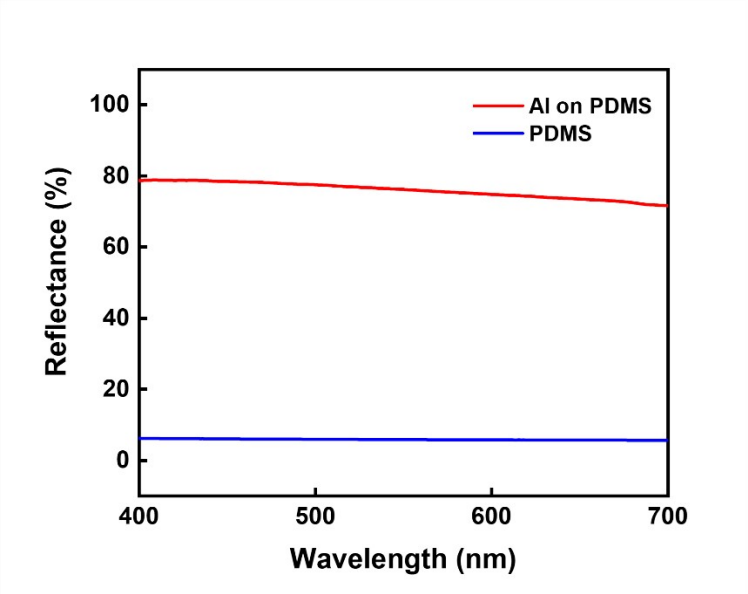

Fig. S6 Reflectance spectra of Al-coated PDMS (red) and bare PDMS (blue).

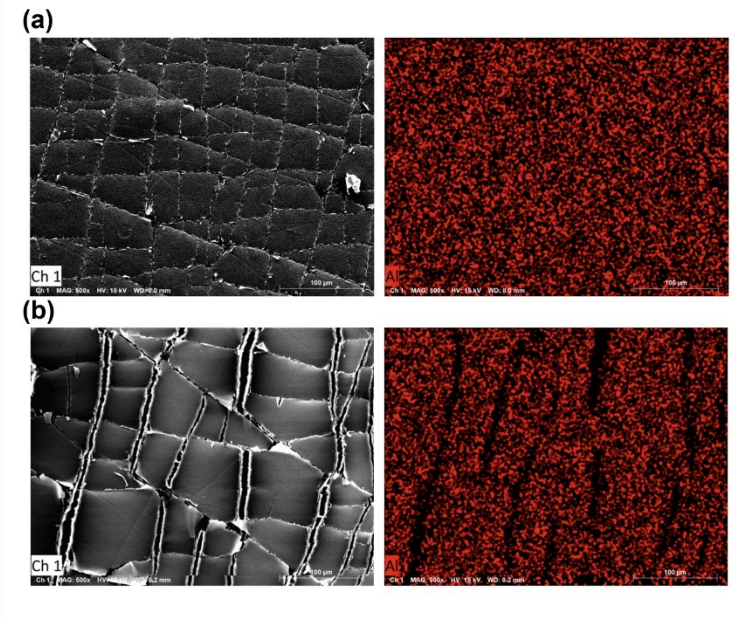

Fig. S7 (a) Scanning electron microscopy (SEM) image and energy-dispersive X-ray spectroscopy (EDS) analysis image under static condition. (b) SEM image and EDS analysis image under stretching conditions.

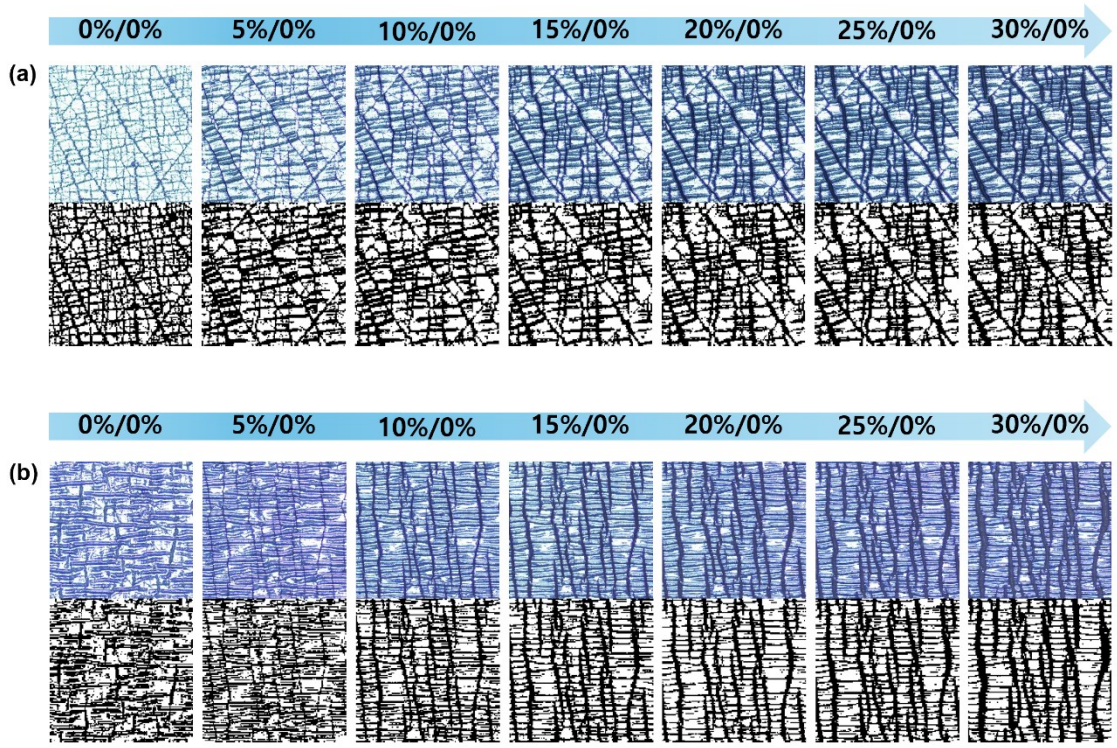

Fig. S8 (a) OM and digital images according to x-axis tensile strain (0–30%) for the UVO 20 min sample. (b) OM and digital images according to x-axis tensile strain (0–30%) for the UVO 30 min sample.

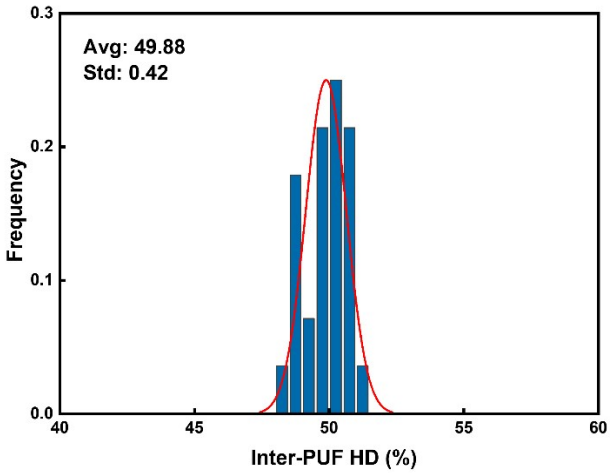

Fig. S9 Inter-PUF HD distribution among eight distinct PUF chips fabricated under identical randomness-encoding conditions.

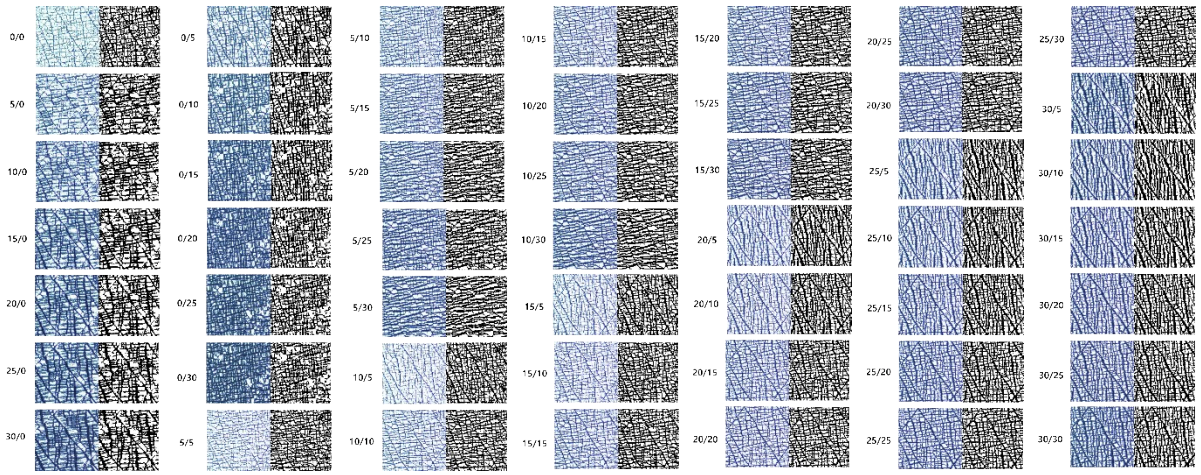

Fig. S10 OM and digital images of challenge-response pairs (CRPs) in the optimized PUF sample for 49 different tensile strain conditions.

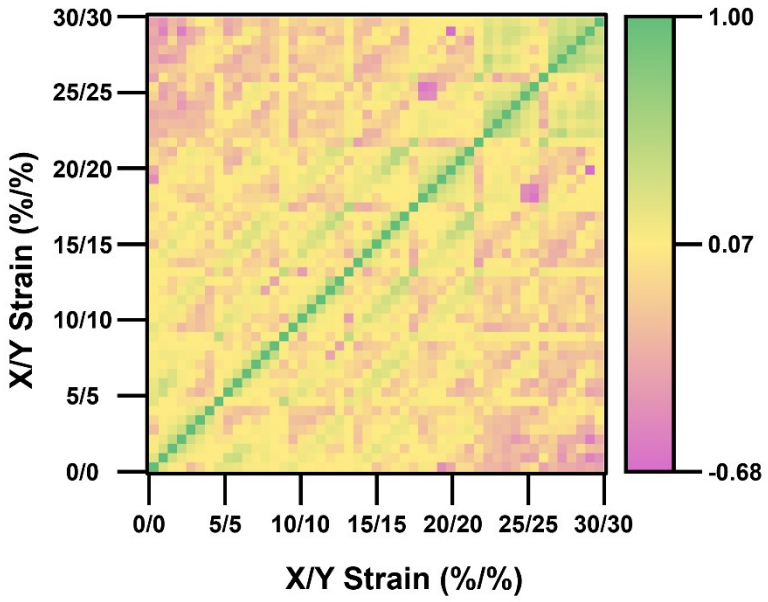

Fig. S11 49 × 49 Pearson correlation coefficient (PCC) heatmap for pairwise comparison across all 49 CRPs.

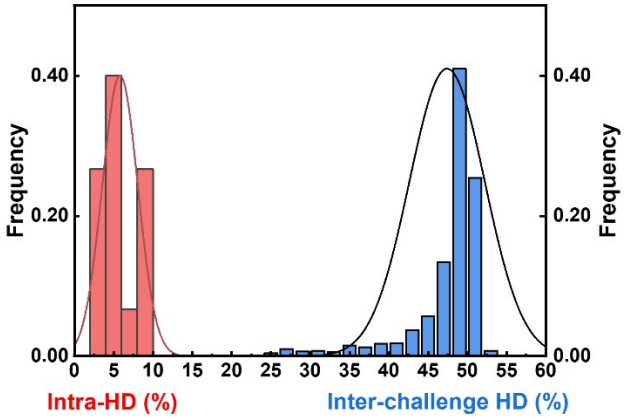

Fig. S12 Distributions of hamming distance for intra-HD (red) and inter-challenge HD (blue).

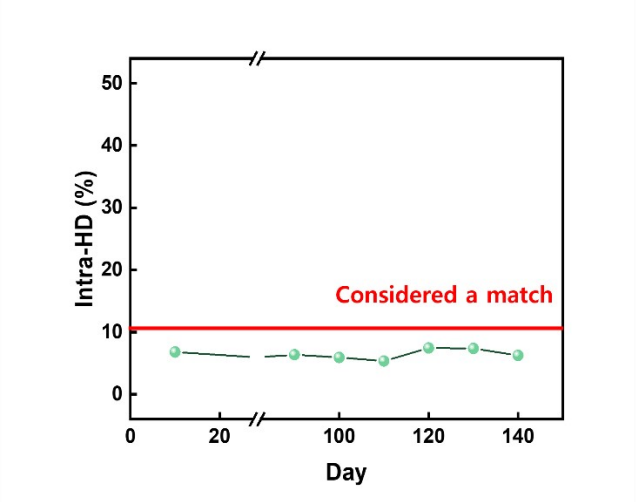

Fig. S13 Intra-HD values measured over a total period of 140 days under ambient conditions.

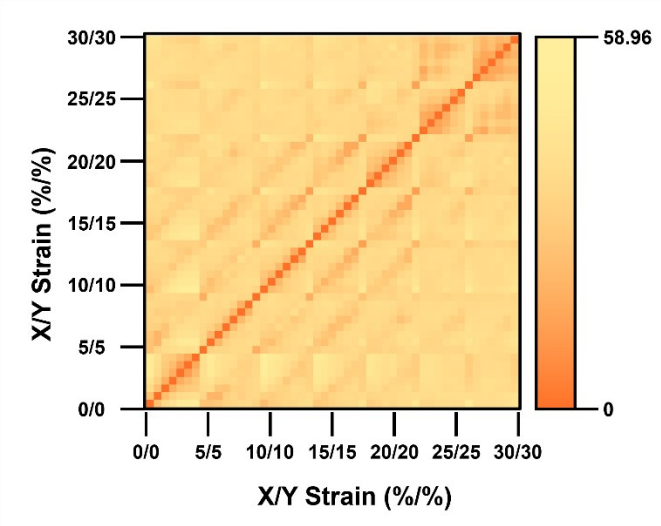

Fig. S14 49 × 49 inter-challenge HD heatmap for pairwise comparison across all 49 CRPs after applying the scale-invariant feature transform (SIFT)-based alignment algorithm.

Angle (°)	Uniformity (%)		Entropy		Inter-HD (%)	
	Average	Standard Deviation	Average	Standard Deviation	Average	Standard Deviation
0	49.77	7.36	0.98	0.02	48.70	6.78
1	49.54	7.63	0.98	0.03	48.81	6.73
2	49.38	7.57	0.98	0.03	48.66	6.64
3	49.98	7.52	0.98	0.02	48.73	6.78
4	49.47	7.20	0.98	0.02	48.60	6.66
5	49.33	7.34	0.98	0.03	48.66	6.53
6	49.37	7.60	0.98	0.03	48.90	6.52
7	49.59	6.65	0.99	0.02	49.09	6.47
8	49.74	5.11	0.99	0.01	49.18	6.43
9	49.47	5.12	0.99	0.01	49.18	6.44
10	49.95	5.55	0.99	0.01	49.18	6.43
11	49.74	5.77	0.99	0.01	49.41	6.34
12	49.56	5.47	0.99	0.01	49.51	6.33
13	49.95	5.70	0.99	0.01	49.60	6.26
14	49.99	5.77	0.99	0.01	49.50	6.31
15	49.93	5.67	0.99	0.01	49.42	6.20
16	49.89	5.20	0.99	0.01	49.55	6.21
17	49.62	5.45	0.99	0.01	49.50	6.23
18	49.90	5.28	0.99	0.01	49.60	6.16
19	49.74	5.47	0.99	0.01	49.73	6.21
20	49.98	5.80	0.99	0.02	49.71	6.23
21	49.73	5.64	0.99	0.02	49.65	6.20
22	49.45	5.85	0.99	0.01	49.52	6.19
23	49.51	5.58	0.99	0.01	49.53	6.15
24	49.55	5.09	0.99	0.01	49.66	6.25
25	49.86	5.66	0.99	0.01	49.54	6.25
26	49.77	5.90	0.99	0.02	49.53	6.39
27	49.74	6.14	0.99	0.02	49.54	6.37
28	49.90	5.80	0.99	0.02	49.62	6.27
29	49.31	6.06	0.99	0.02	49.71	6.31
30	49.93	5.64	0.99	0.01	49.88	6.23
31	49.85	5.15	0.99	0.01	49.96	6.19
32	49.43	4.85	0.99	0.01	50.05	6.24
33	49.82	5.40	0.99	0.01	49.98	6.24
34	49.49	5.24	0.99	0.01	49.89	6.23
35	49.47	5.02	0.99	0.01	49.91	6.29
36	49.72	5.23	0.99	0.01	49.84	6.19
37	49.87	5.36	0.99	0.01	49.99	6.36
38	49.88	5.38	0.99	0.01	49.97	6.36
39	49.88	5.28	0.99	0.01	50.04	6.42
40	49.84	5.41	0.99	0.01	50.07	6.43
41	49.93	5.24	0.99	0.01	50.05	6.43
42	49.49	5.02	0.99	0.01	50.07	6.34
43	49.74	4.93	0.99	0.01	50.01	6.31
44	49.93	5.33	0.99	0.01	50.03	6.44
45	49.91	5.59	0.99	0.02	50.07	6.57
46	49.69	6.02	0.99	0.01	50.04	6.43
47	49.65	6.02	0.99	0.01	50.03	6.40
48	49.80	6.16	0.99	0.01	50.04	6.50
49	49.53	5.73	0.99	0.01	50.05	6.29
50	49.80	5.63	0.99	0.01	50.02	6.30
51	49.79	5.57	0.99	0.01	49.99	6.30

52	49.68	5.76	0.99	0.02	50.07	6.23
53	49.53	5.24	0.99	0.01	49.96	6.23
54	49.63	5.39	0.99	0.01	50.01	6.25
55	49.32	5.61	0.99	0.01	49.97	6.20
56	49.98	5.38	0.99	0.01	49.92	6.19
57	49.41	5.50	0.99	0.01	49.81	6.22
58	49.52	5.29	0.99	0.01	49.82	6.22
59	49.72	5.07	0.99	0.01	49.93	6.20
60	49.58	5.20	0.99	0.01	49.81	6.22
61	49.86	5.06	0.99	0.01	49.83	6.26
62	49.64	5.33	0.99	0.01	49.95	6.18
63	49.69	5.52	0.99	0.01	49.86	6.30
64	49.77	6.13	0.99	0.02	49.65	6.24
65	49.90	5.79	0.99	0.01	49.31	6.14
66	49.78	5.93	0.99	0.01	49.34	6.13
67	49.54	6.10	0.99	0.01	49.51	6.21
68	49.77	6.70	0.99	0.02	49.61	6.36
69	49.95	6.77	0.99	0.02	49.76	6.36
70	49.82	6.66	0.99	0.02	49.79	6.32
71	49.52	7.04	0.99	0.02	49.82	6.35
72	49.72	7.25	0.99	0.02	49.68	6.35
73	49.54	7.52	0.98	0.02	49.74	6.39
74	49.41	7.38	0.98	0.02	49.73	6.45
75	49.57	7.16	0.98	0.02	49.84	6.52
76	49.55	7.17	0.99	0.02	49.96	6.60
77	49.57	7.49	0.99	0.02	49.96	6.61
78	49.64	8.61	0.98	0.02	49.91	6.77
79	49.82	6.66	0.98	0.03	49.89	6.61
80	49.80	8.38	0.98	0.03	50.01	6.71
81	49.58	9.10	0.98	0.03	49.84	6.71
82	49.99	9.77	0.97	0.04	49.82	6.75
83	49.49	9.21	0.98	0.04	49.78	6.69
84	49.22	9.25	0.97	0.04	49.79	6.68
85	49.51	10.11	0.97	0.05	49.68	6.66
86	49.44	11.11	0.96	0.06	49.41	6.68
87	49.83	11.51	0.96	0.07	49.20	6.82
88	49.57	10.92	0.96	0.05	49.36	6.85
89	49.33	9.80	0.97	0.03	49.36	6.75

Table S1. Inter-HD, uniformity, and entropy of the optical PUF patterns generated from the region of interest (ROI) rotation.

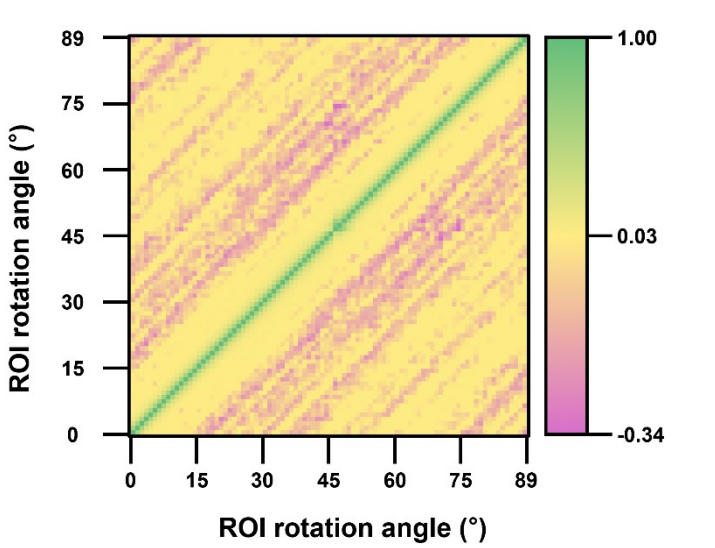

Fig. S15 90 × 90 Pearson correlation coefficient (PCC) heatmap for pairwise comparison across all 90 region of interest (ROI) reconfigurations.

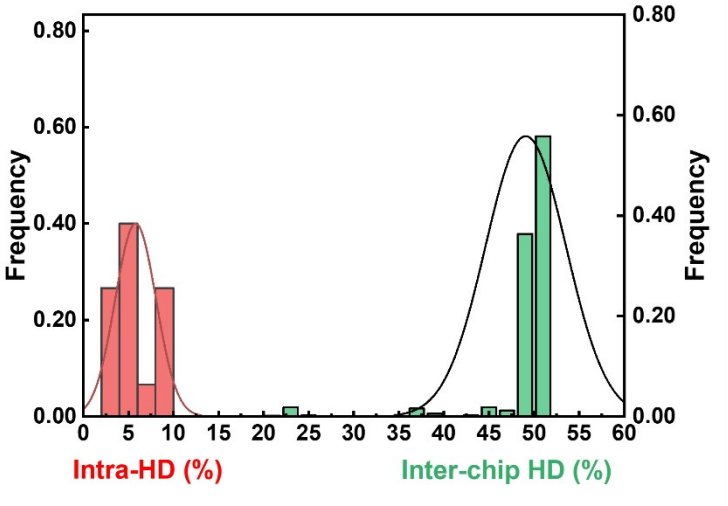

Fig. S16 Distributions of hamming distance for intra-HD (red) and inter-chip HD (green).

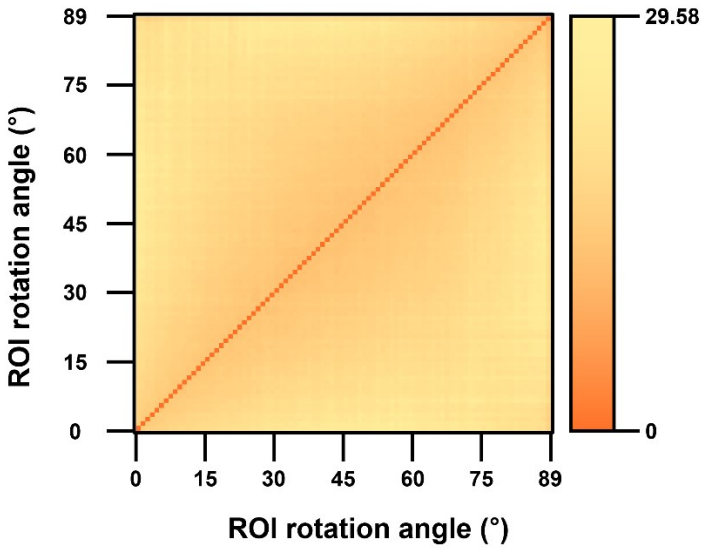

Fig. S17 90 × 90 inter-chip HD heatmap for all 90 readout-level reconfigurations after applying the SIFT-based alignment algorithm.

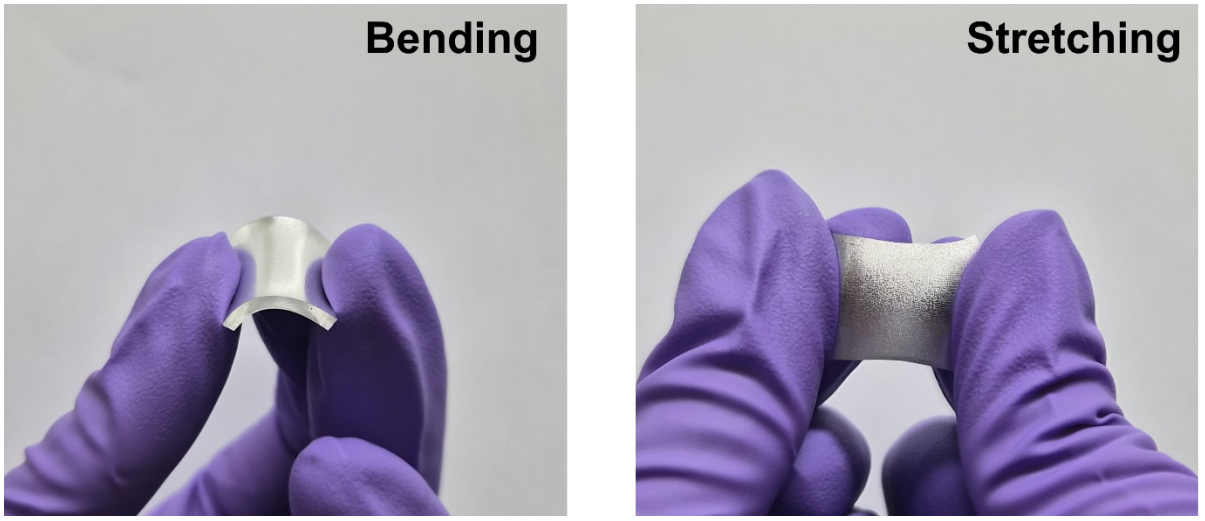

Fig. S18 Photographs showing mechanical actuation of the optical PUF by bending (left) and stretching (right).

Material	Origin of randomness	Challenge expansion	Expansion method	Reconfigurability	Reconfiguration method	Ref
Chiral liquid crystal	Surface wrinkles	O	Optical (polarization)	X	-	[1]
Chiral liquid crystal	Right/Left Chiral domain	O	Optical (polarization)	X	-	[2]
Au nanoparticle	Distribution nonuniformity	O	Optical (wavelength, polarization))	X	-	[3]
Au nanoparticle	Distribution nonuniformity	O	Optical (wavelength)	X	-	[4]
InP/ZnS quantum dot	Distribution nonuniformity	O	Optical (intensity)	X	-	[5]
Au Thin Film	Random fractal network	X	-	X	-	[6]
VO_2 nanocrystal	Distribution nonuniformity	X	-	O	Heating (w/ extra hardware)	[7]
Liquid crystal	Distribution nonuniformity	O	Optical (patterned light)	O	Heating (w/ extra hardware)	[8]
Liquid crystal	Distribution nonuniformity	O	Logical (XOR masking)	O	Heating (w/ extra hardware)	[9]
$Ge_2Sb_2Te_5$	Grain-size nonuniformity	O	Optical (position multiplexing)	O	Heating (w/ extra hardware)	[10]
PDMS	Surface wrinkles	O	Mechanical (strain-vector)	O	ROI rotation (w/o extra hardware)	This work

Table S2. Summary of the characteristics of the optical PUFs including our device (material, origin of randomness, presence of challenge expansion, method, presence of reconfigurability and reconfiguration method).

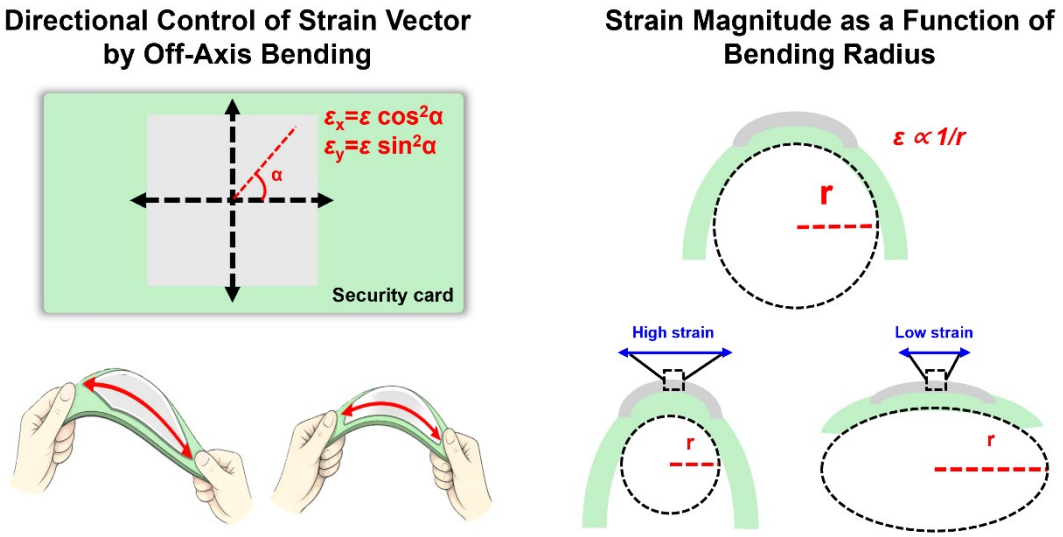

Fig. S19 Card-type optical PUF concept for applying predefined tensile-strain challenges via controlled bending. The strain vector is tuned by bending orientation (α), and the strain magnitude is set by the predefined bending radius (r).

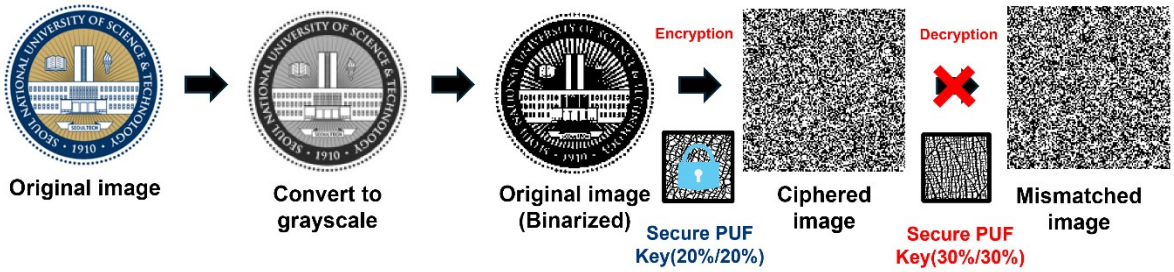

Fig. S20 Result and processing when decrypting the image with a key other than the key used for encryption

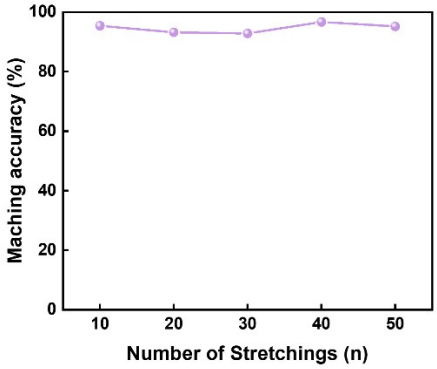

Fig. S21 Image matching accuracy as a function of the number of stretching cycles, quantified as the pixel-level similarity between the decrypted image and the original image.

x-axis/*y*-axis stretching (%/%)	Matching Accuracy (%)
0/0	50.35
0/5	50.19
0/10	50.20
0/15	50.21
0/20	50.84
0/25	49.12
0/30	49.96
5/0	50.22
5/5	50.05
5/10	50.44
5/15	50.07
5/20	49.64
5/25	49.65
5/30	49.83
10/0	49.08
10/5	49.96
10/10	50.18
10/15	49.71
10/20	50.28
10/25	50.15
10/30	49.80
15/0	50.13
15/5	49.94
15/10	50.23
15/15	49.43
15/20	50.32
15/25	50.26
15/30	49.54
20/0	49.66
20/5	49.91
20/10	49.69
20/15	49.79
20/25	49.86
20/30	50.28
25/0	50.29
25/5	49.52
25/10	49.37
25/15	50.02
25/20	49.82
25/25	49.93
25/30	50.14
30/0	50.20
30/5	49.98
30/10	49.73
30/15	49.55
30/20	50.06
30/25	49.47
30/30	49.78

Table S3. Matching accuracy between the original image and images decrypted with nonidentical challenge–response-pair (CRP) keys generated by the proposed PUF. The original image was encrypted using the selected CRP under a 20/20 stretching condition.

References

[1] K. Kim, S.-U. Kim, M.-Y. Choi, M. H. Saeed, Y. Kim and J.-H. Na, *Light: Sci. Appl.*, 2023, **12**, 245.

[2] J.-S. Park, J.-J. Lee, Y.-J. Choi, T.-W. Moon, S. Kim, S. Cho, H. Kang, D. H. Kim, J. Park and S.-W. Choi, *ACS Appl. Mater. Interfaces*, 2024, **16**, 7875–7882.

[3] J. Duan, G. Li, Y. Xiong, X. Zhu, Y. Chen, W. Liu, X. Xu, P. P. Shum, Q. Hao and J. Wang, *Adv. Photonics Nexus*, 2025, **4**, 016003.

[4] J.-K. Kwak, C. Moon, S.-G. Im, T. Kang, H. Jeong, B.-S. Moon, H. Kim, S. J. Kwon, S. Kim and D.-H. Kim, *Adv. Mater.*, 2025, 2503976

[5] M. J. Fong, C. S. Woodhead, N. M. Abdelazim, D. C. Abreu, A. Lamantia, E. M. Ball, K. Longmate, D. Howarth, B. J. Robinson, P. Speed and R. J. Young, *Sci. Rep.*, 2022, **12**, 16919.

[6] N. Sun, Z. Chen, Y. Wang, S. Wang, Y. Xie and Q. Liu, *Nat. Commun.*, 2023, **14**, 2185.

[7] Z. Gan, F. Chen, Q. Li, M. Li, J. Zhang, X. Lu, L. Tang, Z. Wang, Q. Shi, W. Zhang and W. Huang, *ACS Appl. Mater. Interfaces*, 2022, **14**, 5785–5796.

[8] S. Nocentini, U. Rührmair, M. Barni, D. S. Wiersma and F. Riboli, *Nat. Mater.*, 2024, **23**, 369–376.

[9] G. Park, Y.-S. Choi, S. J. Kwon and D. K. Yoon, *Adv. Mater.*, 2023, **35**, 2303077.

[10] Y. Yang, R. Hui, X. Lu, L. Tang, Z. Gan, M. Li, J. Zhang, K. Chen, F. Chen and W. Huang, *ACS Photonics*, 2024, **11**, 4691–4699.